Case Study

Mitigation of Vortex-Induced Vibration in Bridges Using Semiactive Tuned Mass Dampers

Jun Dai, S.M.ASCE[1]; Zhao-Dong Xu, A.M.ASCE[2]; Pan-Pan Gai[3]; and Yan-Wei Xu[4]

Abstract: With increases in the span length, the vortex-induced vibration (VIV) in bridges often occurs at modest wind velocities. The tuned mass damper (TMD) is very effective in mitigating the VIV, while robustness is a major concern for the TMD control with a small mass ratio. To improve the robustness, a magnetorheological TMD (MRTMD) instead of the TMD is used to mitigate the VIV with slowly time-varying frequency. A control strategy considering VIV characteristics is proposed for realizing the real-time tuning and mass stroke limitation simultaneously, including the control force design, control command determination, and frequency estimation. Numerical simulations of a long-span continuous bridge subjected to the VIV are presented to validate the feasibility of the control strategy and the superiority of the MRTMD control. Numerical results show that the MRTMD control is more robust against the resonant frequency change than the TMD control, and the maximum mass stroke is less than a preset stroke in both tuned and mistuned cases. **DOI: 10.1061/(ASCE)BE.1943-5592.0001719**. © *2021 American Society of Civil Engineers*.

Author keywords: Vortex-induced vibration; Semiactive tuned mass damper; Magnetorheological damper; Robustness; Control strategy.

Introduction

For the bridge deck with separated flows, the vortices are shed and then result in a wake that periodically impacts the deck, and the resulting oscillation is the vortex-induced vibration (VIV) (Ehsan and Scanlan 1990; Wu and Kareem 2013). The vortex-shedding frequency f satisfies the Strouhal relation (Ehsan and Scanlan 1990), $f = SU/B$, where S = Strouhal number, U = wind velocity, and B = across-flow dimension of the section (Ehsan and Scanlan 1990). A large-amplitude vortex-induced resonance is locked within a wind velocity range when the vortex-shedding frequency approaches a natural frequency of the bridge (Ehsan and Scanlan 1990; Laima et al. 2013; Wu and Kareem 2013; Dai et al. 2019). Although the vortex-induced resonance is not as catastrophic as the flutter, it seriously impacts the fatigue performance of structural components and driving comfort due to the high occurrence at modest wind velocities (Wu and Kareem 2013).

Many bridges experienced the large-amplitude vortex-induced resonance, for example, Kesssock Bridge (Owen et al. 1996), Great Belt East Bridge (Larsen et al. 2000), Rio-Niteroi Bridge (Battista and Pfeil 2000), Trans-Tokyo Bay Bridge (Fujino and Yoshida 2002), Severn Bridge (Macdonald et al. 2002), Xihoumen Bridge (Li et al. 2014), and Jindo Bridge (Kim et al. 2016). Two types of strategies were adopted to mitigate the VIV in bridges: (1) aerodynamic countermeasures; and (2) tuned mass damper (TMD) control. Field test results showed that the TMD is very effective in mitigating the VIV in bridges (Larsen et al. 1995, 2000; Battista and Pfeil 2000; Fujino and Yoshida 2002; Sun et al. 2020). However, the control effect of the TMD is sensitive to the detuning, especially for the TMD with a small mass ratio (Dai et al. 2020b). Considering that the TMD used in bridges has a small mass ratio of less than 1.5% (Larsen et al. 1995, 2000; Battista and Pfeil 2000; Fujino and Yoshida 2002; Dai et al. 2019), the robustness of the TMD control becomes a major concern in the VIV mitigation.

To improve the robustness against the detuning, the designed damping ratio of the TMD is larger than the optimal solution, but the improvement is limited, and the optimal control effect is greatly weakened. Semiactive TMDs proved to be robust enough by adjusting dynamic characteristics of the TMD in real time, such as the magnetorheological TMD (MRTMD) (Weber and Maślanka 2012; Weber 2013a), TMD with variable damping and stiffness (Sun and Nagarajaiah 2014), TMD with variable mass (Shi et al. 2018), and self-adjustable TMD (Wang et al. 2019). Among these semiactive TMDs, the MRTMD has a good control effect even when the resonant frequency shift reaches −12.2% and +10.4%. (Weber and Maślanka 2012). Because MR dampers offer mechanical simplicity, high dynamic range, low power requirements, large force capacity, and robustness (Dyke et al. 1996, 1998; Yang et al. 2002), the MRTMDs were used to suppress various unwanted structural vibrations, such as the harmonic vibration (Maślanka 2019), earthquakes (Zemp et al. 2011; Christie et al. 2019), floor vibration (Setareh et al. 2007), wind-induced vibration (Kang et al. 2011; Weber and Maślanka 2014), and cable vibration (Wu and Cai 2007).

However, few studies have addressed the MRTMD control of the VIV in bridges. Weber (2014) used the MRTMD to suppress the wind-induced vibration of Volgograd Bridge; they focused on the precise tuning of the MRTMD but ignored the effect of VIV characteristics on the control force determination. If the VIV is considered as a harmonic vibration (Weber and Maślanka 2014), the control force and mass stroke of the MRTMD may not be

[1]Key Laboratory of C&PC Structures of the Ministry of Education, Southeast Univ., Nanjing 210096, China. Email: daijun4242@163.com

[2]Professor, Key Laboratory of C&PC Structures of the Ministry of Education, Southeast Univ., Nanjing 210096, China (corresponding author). Email: zhdxu@163.com

[3]Ph.D. Candidate, Key Laboratory of C&PC Structures of the Ministry of Education, Southeast Univ., Nanjing 210096, China. Email: gaipan100@163.com

[4]Ph.D. Candidate, Key Laboratory of C&PC Structures of the Ministry of Education, Southeast Univ., Nanjing 210096, China. Email: 230179426@seu.edu.cn

Note. This manuscript was submitted on June 14, 2020; approved on January 14, 2021; published online on March 25, 2021. Discussion period open until August 25, 2021; separate discussions must be submitted for individual papers. This paper is part of the ***Journal of Bridge Engineering***, © ASCE, ISSN 1084-0702.

reasonably designed in the absence of measurement data from real bridges. Because the mass ratio of the TMD used in bridges is small, the mass stroke of the TMD is large for realizing the vibration energy absorption (Fujino and Yoshida 2002). Furthermore, the stroke capability of existing MR dampers cannot meet the mass stroke demand of the TMD (Zemp et al. 2016). Thus, the mass stroke limitation becomes a design concern of the MRTMD control. Because the VIV has self-limiting characteristics (Ehsan and Scanlan 1990; Larsen 1995; Wu and Kareem 2013), the mass stroke of the MRTMD can be predicted according to the wind tunnel test result and the VIV model. In our opinion, the control force design of the MRTMD should consider the control effect and mass stroke limitation, simultaneously.

The dominant frequency plays an important role in determining the semiactive control force of the MRTMD. As a result, the frequency estimation should be real time, accurate, and robust to the measurement noise. The common frequency estimation methods are the short-time Fourier transform (Nagarajaiah and Varadarajan 2005), Hilbert transform (Nagarajaiah 2009), zero-crossings recording (Weber 2013b), and so on. It is noted that, at the beginning of the MRTMD control, the sensors and controller take time to collect data and estimate the dominant frequency. If an offline frequency estimation based on long-term monitoring data is applied to the MRTMD control, the MRTMD realizes the tuning as soon as possible.

This study aims at proposing a reliable control strategy for the MRTMD mitigating the VIV in bridges. First, an equivalent damping ratio contributed by TMDs is presented based on the semiempirical nonlinear model. Then, a control strategy that consists of the control force design, control command determination, and frequency estimation is proposed for the MRTMD. Finally, several numerical simulations of a long-span continuous bridge subjected to the VIV are performed to validate the feasibility of the control strategy and the superiority of the MRTMD control.

Vortex-Induced Vibration

The semiempirical nonlinear model proposed by Ehsan and Scanlan (1990) is used to model the vortex-induced force acting on the bridge deck

$$f_v = \frac{1}{2}\rho U^2(2B) \times \left[Y_1(K)\left(1-\varepsilon(K)\frac{y^2}{B^2}\right)\frac{\dot{y}}{U} + Y_2(K)\frac{y}{B} + \frac{1}{2}C_L(K)\sin(\omega t+\theta)\right] \tag{1}$$

where y = displacement of the bridge deck; ρ = air density; U = wind velocity; B = across-flow dimension of the section; Y_1, Y_2, and ε = aerodynamic parameters obtained by wind tunnel tests, respectively; C_L = lift coefficient; θ = initial phase; $K = \omega B/U$ = reduced frequency of vortex-shedding; and ω = vortex-shedding frequency that satisfies the relation, as shown in Fig. 1.

In Fig. 1, the platform segment is the lock-in region where the vortex-shedding frequency is locked when it approaches to a natural frequency of the bridge. Within the lock-in region, the bridge deck resonates with self-excited and self-limited characteristics (Ehsan and Scanlan 1990; Wu and Kareem 2013), so Eq. (1) in the vortex-induced resonance can be simplified as follows:

$$f_v = \frac{1}{2}\rho U^2(2B)Y_1\left(1-\varepsilon\frac{y^2}{B^2}\right)\frac{\dot{y}}{U} \tag{2}$$

The equation of motions of the bridge deck with a TMD under the VIV can be written as follows:

$$\ddot{q}(t) + 2\xi_b\omega_b\dot{q}(t) + \omega_b^2 q(t) = \frac{\rho UBY_1}{M}(\alpha_2 - \bar{\varepsilon}\alpha_4 q(t)^2)\dot{q}(t) - \mu(\ddot{q}(t) + \ddot{q}_t(t)) \tag{3}$$

$$\ddot{q}_t(t) + \ddot{q}(t) + 2\xi_t\omega_t\dot{q}_t(t) + \omega_t^2 q_t(t) = 0 \tag{4}$$

where $q(t)$ and $q_t(t)$ = generalized coordinates of the system, $y(x,\ t) = q(t)\phi(x)$, $y_t(t) = \phi(x_t)q_t(t)$; $\phi(x)$ = mode shape vector of the bridge; $M = \int_0^L \phi(x)^2 m(x)\mathrm{d}x$, ω_b, and ξ_b = generalized mass, natural frequency, and damping ratio of the bridge, respectively; y_t = displacement of the TMD; x_t = coordinate of the installation position of the TMD; $\mu = \phi(x_t)^2 m_t/M$ = mass ratio; m_t, ω_t, and ξ_t = mass, natural frequency and damping ratio of the TMD, respectively; and $\bar{\varepsilon} = \varepsilon/B^2$, $\alpha_2 = \int_0^L \phi(x)^2\mathrm{d}x$, and $\alpha_4 = \int_0^L \phi(x)^4\mathrm{d}x$. Fig. 2(a) shows the bridge-TMD system.

TMD Contribution

Although the time-stepping method can be applied to solve Eqs. (3) and (4), an analytical solution is more welcome to understand the TMD contribution to the VIV mitigation. The Krylov–Bogoliubov method is used to obtain the vortex-induced amplitude of the bridge.

Assume that the steady-state solution of the system can be written as follows:

$$\begin{cases} q(t) = \Lambda_1 e^{i\omega t} \\ q_t(t) = \Lambda_2 e^{i\omega t} \end{cases} \tag{5}$$

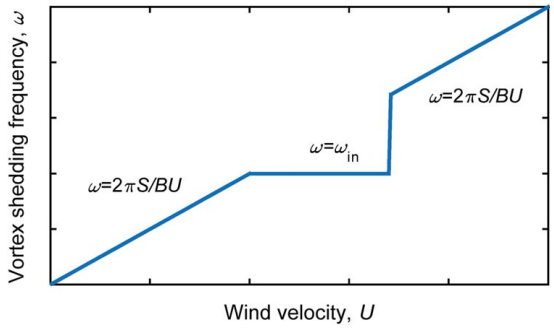

Fig. 1. Vortex-shedding frequency with the wind velocity.

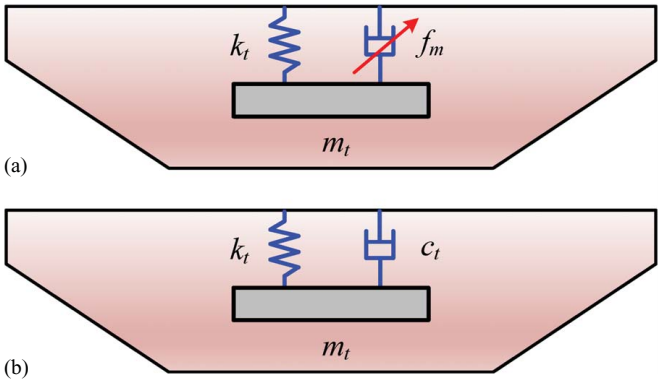

Fig. 2. Bridge-mass damper system: (a) TMD; and (b) semiactive TMD.

where Λ_1 and Λ_2 = complex amplitudes of the bridge and TMD, respectively. According to Eqs. (4) and (5), we can obtain the following relation:

$$\frac{\Lambda_2}{\Lambda_1} = \frac{\gamma^2(\beta^2-\gamma^2)}{(\beta^2-\gamma^2)^2+(2\xi_t\beta\gamma)^2} + \frac{-\gamma^2(2\xi_t\beta\gamma)i}{(\beta^2-\gamma^2)^2+(2\xi_t\beta\gamma)^2} = t_1 + it_2 \quad (6)$$

where $\beta = \omega_t/\omega_b$ = frequency ratio; $\gamma = \omega/\omega_b$ = resonance frequency ratio; and $r = |\Lambda_2/\Lambda_1|$ = stroke-amplitude ratio. Substituting Eq. (6) into Eq. (4) yields

$$\ddot{q}_t(t) = -\omega^2 t_1 q(t) - \omega t_2 \dot{q}(t) \quad (7)$$

Then, the general form of a nonlinear system can be obtained as follows:

$$\ddot{q}(t) + \omega_b^2 q(t) = f(\dot{q}, q, t) \quad (8)$$

where $f(\dot{q}, q, t)$ can be written as follows:

$$f(\dot{q}, q, t) = \frac{\rho U B Y_1}{M}(\alpha_2 - \bar{\varepsilon}\alpha_4 q^2(t))\dot{q}(t) + \mu(\omega^2 t_1 q(t) + \omega t_2 \dot{q}(t)) + \mu\omega^2 q(t) - 2\xi_b\omega_b\dot{q}\ (t) \quad (9)$$

According to the Krylov–Bogoliubov method, the two equations can be obtained as follows:

$$\frac{\rho U B Y_1}{4M}\bar{\varepsilon}\alpha_4 a^2 + 2\xi_b\omega_b - \mu\omega t_2 - \frac{\rho U B Y_1}{M}\alpha_2 = 0 \quad (10)$$

$$\gamma^6 - (2\beta^2 - 4\xi_t^2\beta^2 + 1 + \mu\beta^2 - 4\mu\xi_t^2\beta^2)\gamma^4 + (\beta^4 + 2\beta^2 - 4\xi_t^2\beta^2 + \mu\beta^4)\gamma^2 - \beta^4 = 0 \quad (11)$$

The resonance frequency ratio γ can be obtained by solving Eq. (11). The vortex-induced amplitude can be obtained by solving Eq. (10)

$$a = 2\sqrt{\frac{\alpha_2}{\bar{\varepsilon}\alpha_4}}\sqrt{1 - \frac{2M\omega_b(\xi_b + \xi_e)}{\alpha_2\rho U B Y_1}} \quad (12)$$

$$\xi_e = \frac{\mu\xi_t\beta\gamma^4}{(\beta^2-\gamma^2)^2+(2\xi_t\beta\gamma)^2} \quad (13)$$

where ξ_e = equivalent damping ratio contributed by the TMD. The smallest ξ_e is considered as the stable equivalent damping ratio due to the existence of triple solutions in Eq. (11) in some cases (Dai et al. 2020a). It is noted that the vortex-induced resonance is eliminated when $\xi_b + \xi_e$ is larger than ξ_c that satisfies $2M\omega_b\xi_c = \alpha_2\rho U B Y_1$; in other words, there is no steady-state solution for the nonlinear system in this case.

To evaluate the accuracy of the approximate analytical solution, Fig. 3 shows the comparison between the exact result and the approximate analytical result. Wind tunnel test data from a sectional model (Liao 2013; Qin et al. 2013) are used to identify aerodynamic parameters: $\rho U B Y_1/M = 0.102$, $\bar{\varepsilon} = 143.35$, and $\xi_c = 1\%$. Sectional model parameters are $\alpha_2 = \alpha_4 = 1$, $\omega_b = 0.806$ Hz, and $\xi_b = 0.3\%$ (Liao 2013; Qin et al. 2013). TMD parameters are $\mu = 0.3\%$, $\beta = [0.95, 0.97, 1, 1.03, 1.05]$, and $\xi_t = [3\%, 5\%, 8\%]$. The initial amplitude of the bridge is assumed as 50 mm. The Runge–Kutta time-stepping method is applied to calculate the exact time–domain response.

The vortex-induced resonance is mitigated and eliminated when $\beta = 0.95$, 1.05 and $\beta = 0.97$, 1, 1.03, respectively. $r = q_{t,\max}/q_{\max}$ and $\xi_{\text{eff}} = \xi_c + \xi$ are used as the exact results, $r = |\Lambda_2/\Lambda_1|$ and $\xi_{\text{eff}} = \xi_e + \xi_b$ are used as the approximate analytical results when the resonance is eliminated, i.e., there is no steady-state solution, where $q_{\max}$ = maximum displacement of the bridge; $q_{t,\max}$ = maximum stroke of the TMD; ξ_{eff} effective damping ratio of the bridge; $\xi = \sum_{n=1}^{N}(A_n - A_{n+1})/(2\pi N A_{n+1})$ = apparent damping ratio of the bridge; A_n = nth positive peak of the amplitude; and N = number of the positive peak. The comparison result indicates that the approximate analytical solution can well predict responses of the bridge-TMD system whether the resonance is mitigated or eliminated. Although the errors are relatively large in the two cases: $\beta = 1$ and $\xi_t = 3\%$, and $\beta = 1$ and $\xi_t = 5\%$, the result can be acceptable for the TMD design. In the following section, the equivalent damping ratio and the stroke-amplitude ratio are used to design the desired semiactive control force.

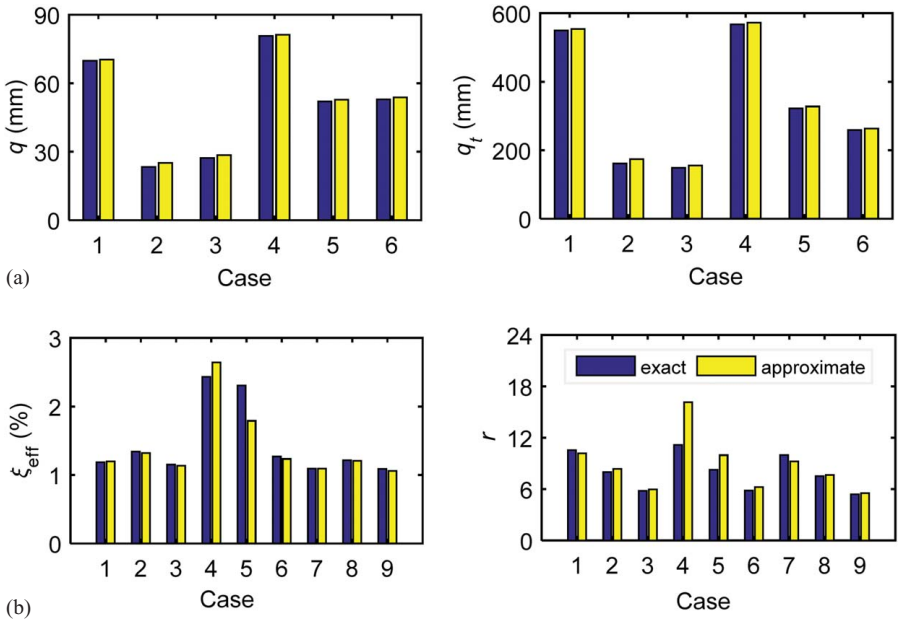

Fig. 3. Comparison between the exact result and the approximate analytical result: (a) mitigated case; and (b) eliminated case.

Control Strategy

In order to improve the robustness and reduce the mass stroke, viscous dampers in the TMD are replaced by MR dampers, as shown in Fig. 2(b). Eq. (4) can be rewritten as follows:

$$\ddot{q}_t(t) + \ddot{q}(t) + f_s(\dot{q}_t, q_t, t) + \omega_t^2 q_t(t) = 0 \tag{14}$$

where f_s = semiactive control force provided by MR dampers. The control strategy includes the control force design, control command determination, and frequency estimation.

Control Force Design

The damping ratio of the MRTMD is determined by considering the stroke capacity of the MR damper and robustness, simultaneously. The robustness refers to the ability of the MRTMD or TMD to maintain a good control effect under the structural parameter uncertainty. The structural parameter uncertainty refers to the uncertainty in the generalized stiffness for the controlled mode of the bridge.

Fig. 4 shows the equivalent damping ratio and stroke-amplitude ratio with varying TMD parameters when $\mu = 0.3\%$. In Fig. 4, the equivalent damping ratio characterizes the control effect of the TMD, and the frequency ratio change characterizes the generalized stiffness uncertainty. When the equivalent damping ratio is given, the damping ratio ξ_t with the widest range of β is optimal for the robustness. It can be seen from Fig. 4(a) that an optimal ξ_t exists for the robustness, taking the model (Liao 2013; Qin et al. 2013), for example, the optimal ξ_t is 5% by assuming the designed equivalent damping ratio to be 1%. Because the damping can weaken the motion of the auxiliary mass, the stroke-amplitude ratio decreases with the increase of ξ_t. According to the *Wind-resistant design specification for highway bridges* (JTG/T 3360-01-2018, Ministry of Communication of PRC 2019), the vortex-induced resonant amplitude of the bridge should be smaller than $0.04/f_v$ (unit: meter), where f_v = vertical vibration frequency. The estimated resonance frequency of the bridge is 0.806 Hz, so the limit is 50 mm. The MR damper with a stroke capacity of 300 mm (Fujitani et al. 2008) is used in numerical simulations. Based on these, the stroke-amplitude ratio should be between 7 and 8, i.e., $\xi_t = 5\% - 7\%$. The damping ratio of the MRTMD is 6% by weighting the equivalent damping ratio and the stroke-amplitude ratio.

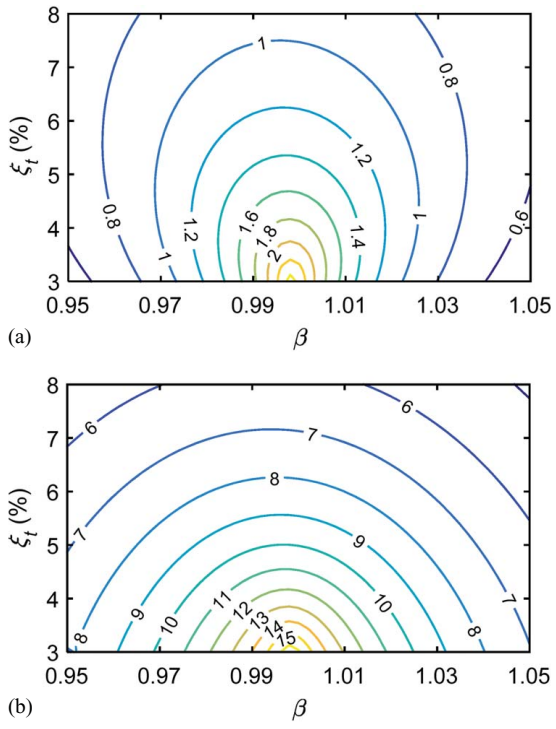

Fig. 4. Equivalent damping ratio and stroke-amplitude ratio with TMD parameters when $\mu = 0.3\%$: (a) equivalent damping ratio; and (b) stroke-amplitude ratio.

The frequency ratio is determined by maximizing the equivalent damping ratio, $\max\{\xi_e(\beta_{\text{opt}}, \xi_t, \mu,)\}$. Fig. 5 shows the equivalent damping ratio with varying frequency ratio. The optimal frequency ratio is 0.996 by picking the peak of the equivalent damping ratio, 1.25%.

Finally, the desired control force can be determined by

$$f_d(\dot{q}_t, q_t, t) = m_t\beta_{\text{opt}}^2(\omega_b^2 - \bar{\omega}_b^2)q_t(t) + 2m_t\xi_t\beta_{\text{opt}}\omega_b\dot{q}_t(t) \tag{15}$$

where $\bar{\omega}_b$ = estimated natural frequency of the bridge in the design phase; and ω_b = natural frequency of the real bridge. Due to the existence of modeling errors, the natural frequency of the real bridge differs from the estimated value. Although TMD parameters can be adjusted after installation, the detuning may occur due to environmental effects and traffic variability. Thus, the MR damper should weaken the detuning as much as possible by providing the desired control force in Eq. (15).

Control Command Determination

However, the desired control force cannot be perfectly provided by the MR damper, because the MR damper force and the relative velocity at both ends have the same sign, i.e., the clipped property of the MR damper force (Dyke et al. 1996, 1998). Besides, the control force provided by the MR damper cannot be directly commanded, only the control voltage V applied to the current driver (Dyke et al. 1996, 1998). There are three types of MR damper force control schemes: feed-forward control, feedback control, and combined control (Weber 2013a). A feed-forward control named the piecewise linear interpolation is used to determine the control voltage. Its accuracy and real-time performance were validated by simulations and experiments (Weber 2013a).

The piecewise linear interpolation scheme considering the clipped property can be expressed as follows:

$$V = \begin{cases} V_n + \dfrac{f_d - f_s(V_n)}{f_s(V_{n+1}) - f_s(V_n)}, & \dot{q}_t f_d \geq 0 \text{ and } |f_s(V_{n+1})| < |f_d| \leq |f_s(V_n)| \\ V_N, & \dot{q}_t f_d \geq 0 \text{ and } |f_d| > |f_s(V_N)| \\ 0, & \dot{q}_t f_d < 0 \end{cases} \tag{16}$$

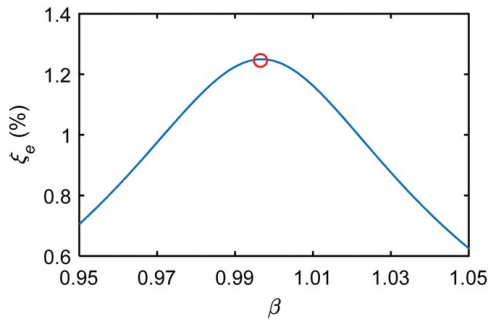

Fig. 5. Equivalent damping ratio with the frequency ratio.

where $f_s(V_n)$ = MR damper force estimated by the MR damper model when the control voltage is V_n. The control voltage is divided into $N+1$ levels: 0, V_1, V_2, …, V_n, …, V_N, and the difference between levels is ΔV, $V_{n+1} = V_n + \Delta V$.

To obtain the desired control force and MR damper force, the relative velocity and relative displacement at both ends of the MR damper should be known. The kinematic Kalman filter (KKF) (Jeon and Tomizuka 2007) is applied to estimate the denoised $\dot{q}_t$ and q_t. The measurements are (1) the accelerations of the bridge and TMD; and (2) the stroke of the TMD. The KKF can be expressed by the following two equations:

$$\begin{Bmatrix} \dot{x}_1 \\ \dot{x}_2 \end{Bmatrix} = \begin{bmatrix} 0 & 1 \\ 0 & 0 \end{bmatrix} \begin{Bmatrix} x_1 \\ x_2 \end{Bmatrix} + \begin{bmatrix} 0 \\ 1 \end{bmatrix} u + \begin{bmatrix} 0 \\ 1 \end{bmatrix} w \tag{17}$$

$$y_k = \begin{bmatrix} 1 & 0 \end{bmatrix} \begin{Bmatrix} x_1 \\ x_2 \end{Bmatrix} + v \tag{18}$$

where x_1 and x_2 = states of the KKF; and y_k = measurement of the KKF. In the bridge-MRTMD system, x_1 and $x_2 = q_t$ and $\dot{q}_t$; u = measured relative acceleration $\ddot{q}_t$; w = acceleration measurement noise; y_k = measured stroke of the TMD; and v = displacement measurement noise.

Fig. 6 shows the relative velocity estimated by the KKF. As a comparison, the difference in the relative displacement processed by a low-pass filter is used to estimate the relative velocity. The measurement noise standard deviations are assumed to be 5% of the measurement standard deviations. A good match is observed between the relative velocity estimated by the KKF and the true relative velocity, but the estimation accuracy of the difference method is not good enough.

Frequency Estimation

According to Eq. (15), the natural frequency of the true bridge, ω_b, should be estimated. In our study, the vertical acceleration response of the bridge deck is measured, and a two-step strategy is used to deal with the acceleration measurement for ω_b estimation.

The modal identification of the long-span bridge becomes challenging due to the modal overlapping induced by close-mode characteristics (Xu et al. 1997; Siringoringo and Fujino 2007; Magalhães et al. 2007; Wen et al. 2018). The analytical mode decomposition (AMD) was proposed by Chen and Wang (2012) to improve the modal identification accuracy of close-mode structures, and its superiority over other methods was validated through the simulation, experiment, and field test (Chen and Wang 2012; Wang and Chen 2014; Wen et al. 2018). Thus, the AMD method using the long-term acceleration measurement is adopted to realize a reliable estimation of ω_b at the beginning of the MRTMD control.

According to the AMD, a signal $s(t)$ can be decomposed into m signals $s_i(t)$ with the independent Fourier spectrum

$$s(t) = \sum_{i=1}^{m} s_i(t) \tag{19}$$

Each signal $s_i(t)$ has a narrow frequency band and can be expressed as follows:

$$s_i(t) = z_i(t) - z_{i-1}(t),\ \ldots,\ s_n(t) = s(t) - z_{n-1}(t) \tag{20}$$

$$z_i = \sin(\omega_{\text{bis},i}t)H[s(t)\cos(\omega_{\text{bis},i}t)] - \cos(\omega_{\text{bis},i}t)H[s(t)\sin(\omega_{\text{bis},i}t)],\quad i = 1, 2, \ldots, m-1 \tag{21}$$

where $\omega_{\text{bis},i} = i$th bisecting frequency; $z_0 = 0$; and $H[\cdot]$ = Hilbert transform. $\omega_{\text{bis},i}$ can be selected as $(\omega_i + \omega_{i+1})/2$, where $\omega_i = i$th peak frequency of $S(\omega)$; and $S(\omega)$ = Fourier spectrum of $s(t)$.

However, the AMD method is time-consuming and cannot realize an online frequency estimation. After a Δt (Δt = window time) or more, a window method incorporating the fast Fourier transform (FFT) (Shi et al. 2014) is employed to estimate the dominant frequency of the VIV. The latest acceleration induced by the VIV is processed by the window method to obtain its dominant frequency, which is considered as the natural frequency of the bridge, ω_b, because the dominant frequency is very close to the natural frequency in the VIV lock-in region (Ehsan and Scanlan 1990; Wu and Kareem 2013). Fig. 7 shows the flowchart of the dominant frequency estimation. A low-pass filter is employed to weaken the noise disturbance by rolling off the high-frequency component. The window time includes the updating time Δt_1 and overlap time Δt_2, $\Delta t = \Delta t_1 + \Delta t_2$. The updating time means the updating time of desired control force.

Control Strategy Implementation

When the MRTMD works during the VIV, the control voltage is prepared according to the AMD method and then is determined according to the window method after a Δt or more. It is noted that the acceleration and wind velocity measurements are necessary to help judge the existence of the VIV. The large-amplitude vibration at the lock-in wind velocity region is considered as the VIV. The amplitude and lock-in region are determined based on the wind tunnel test or long-term monitoring results. Even if the VIV judgment is not accurate, the proposed control strategy still works. Because the wind-induced vibrations in bridges have a narrow frequency band, the MRTMD which is tuned to the dominant vibration

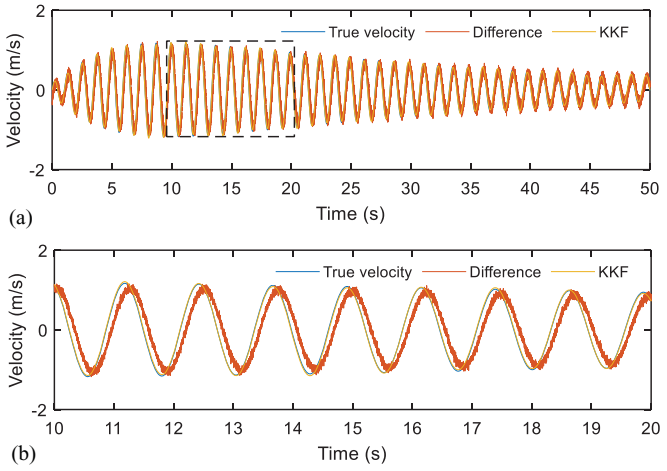

Fig. 6. Estimation result of the relative velocity using the KKF: (a) 0–50 s; and (b) 10–20 s.

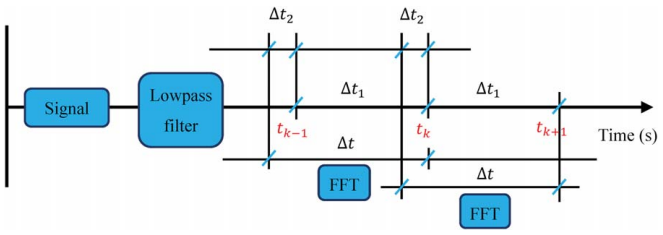

Fig. 7. Dominant frequency estimation of the VIV in bridges.

frequency can effectively mitigate the vibration with a narrow frequency band (Weber 2013b, 2014). Fig. 8 summarizes the control strategy for the bridge-MRTMD system subjected to the VIV, where $\mathbf{y}$ is the measurement vector of the system, t_0 is the starting time of the MRTMD operation, and $\bar{\mathbf{y}}$ includes the processed measurement and estimated velocity.

Numerical Example

6 × 110 m Continuous Bridge

Wind tunnel sectional model tests of a 6 × 110 m continuous bridge (Liao 2013; Qin et al. 2013) showed that the bridge experiences a vertical-bending vortex-induced resonance at wind velocities of 27–35 m/s, with a maximum amplitude of 140 mm. According to the wind tunnel test result, the aerodynamic parameters are identified as $\rho UBY_1/M = 0.102$ and $\bar{\varepsilon} = 143.35$. The details of the finite-element model can be found in our previous work (Dai et al. 2019). The finite-element analysis showed that the natural frequency of the first vertical-bending mode is 0.803 Hz and $\alpha_4/\alpha_2 = 0.75$. Fig. 9 shows the first vertical-bending mode shape of the bridge. The damping ratio for the first vertical-bending mode is assumed to be 0.3%.

Fig. 10 shows the simulated vortex-induced resonance of the bridge with the initial displacement, 50 and 200 mm. It can be seen that the steady-state amplitudes are both 160 mm at the two initial conditions, indicating that the semiempirical nonlinear model described by Eq. (2) can capture the self-excited and self-limited characteristics of the VIV. According to the *Wind-resistant design specification for highway bridges* (Ministry of Communication of PRC 2019), the maximum amplitude of the bridge should be less than 50 mm. Based on the wind tunnel test result (Liao 2013; Qin et al. 2013), the VIV with the first vertical-bending mode is effectively mitigated when the damping ratio of the bridge is larger than 1%. In our simulations, the MRTMD and TMD controls are adopted for the VIV mitigation.

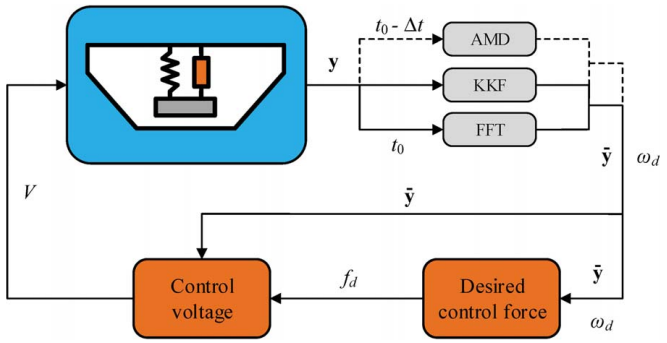

Fig. 8. Control block diagram for the bridge-MRTMD system.

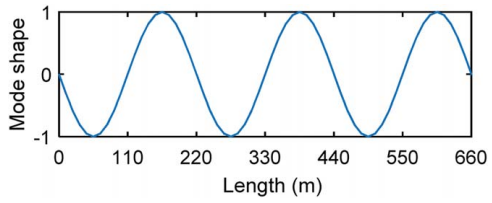

Fig. 9. First vertical-bending mode of the bridge.

Long-Stroke MR Damper

A long-stroke MR damper developed by Fujitani et al. (2008) is used in the example, the maximum force, current, and stroke are 10 kN, 5 A, and 300 mm, respectively. The Bingham plastic model is used to describe the MR damper force, $F = \text{sign}(v)(-219I^2 + 2702I + 611) + 1.90v$, where v = relative velocity of the MR damper. Fig. 11 shows the simulated MR damper force–displacement relationship. A first-order filter is used to describe the dynamics involved in the MR fluid reaching rheological equilibrium (Dyke et al. 1996), $\dot{I} = -\eta(I - V)$, where I and V are the control current and control voltage, and η is assumed as 100.

Ambient Vibration Test

To illustrate the AMD feasibility and mistuning possibility, a simple ambient vibration test was conducted. Two accelerometers (CA-YD-159, Sinocera Piezotronics, Yangzhou city, Jiangsu province, China) were located on the second span to measure the vertical acceleration, as shown in Fig. 12(a). The test was conducted three times. The duration of each test is at least 30 min. The sampling frequency is 20 Hz. Fig. 12(b) shows the measured accelerations of the bridge. Because the bridge was not open to the public and there were a few trucks driving on the bridge during the test, these peaks shown in Fig. 12(b) were caused by driving trucks. Fig. 12(c) shows the Fourier spectrum of Test 1 between 0.4 and 2 Hz.

Wind tunnel tests showed that the vortex-induced resonance behaves as the first vertical-bending mode vibration, thus only the natural frequency for the first vertical-bending mode is identified. Fig. 13 shows the decomposed subsignals of Test 1 and their Fourier spectra using the AMD method. It can be seen that the Fourier spectra are clean, except for the third Fourier spectrum, indicating that subsignals, in general, are well separated. Table 1 presents the identified natural frequencies that are less than 2 Hz. Maybe due to the small ambient excitation or accelerometer location, the identified natural frequency between 1 and 1.3 Hz is ambiguous. Besides, the relative error of −10.58% in the natural frequency for the first vertical-bending mode (0.803 and 0.898 Hz) indicates that the mistuning caused by modeling errors may exist in practice, and an adaptive MRTMD control is needed.

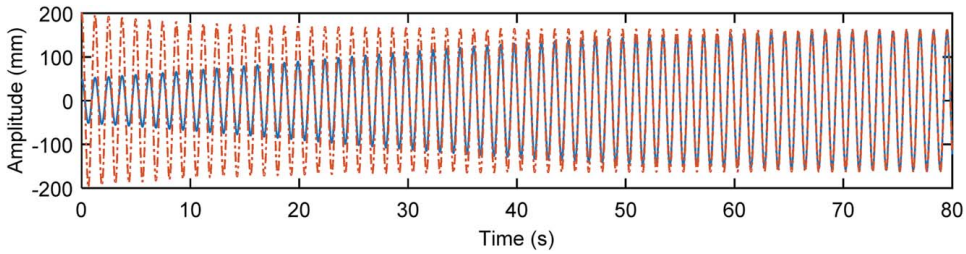

Fig. 10. Vortex-induced resonance of the bridge with the initial displacement of 50 and 200 mm.

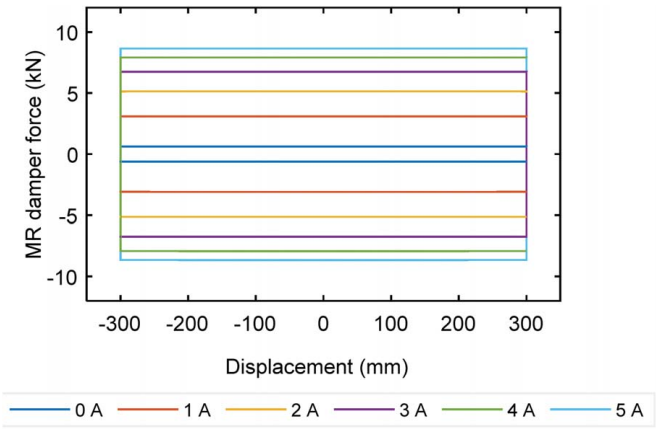

Fig. 11. Simulated MR damper force–displacement relationship.

VIV Mitigation

Three mass ratio cases are considered in the VIV mitigation; $\mu = 0.3\%$, $\mu = 0.5\%$, and $\mu = 1\%$. The frequency ratio and damping ratio of the MRTMD and TMD are determined by considering the control effect and mass stroke limitation, simultaneously. Table 2 presents the design parameters of the MRTMD and TMD.

Comparison between MRTMD Control and TMD Control

Considering that the vortex-induced resonance of the 6×110 m continuous bridge is a low-frequency vibration, the window time Δt is 20 s, the updating time Δt_1 is 5 s, and the overlap time Δt_2 is 15 s. The time interval in simulations is 0.001 s, and the duration is 200 s. The updating time of the control voltage is 0.1 s. The AMD method is used to estimate the natural within the first 20 s. The window method is used to estimate the dominant vibration frequency in the remaining 180 s. The measurement noise standard

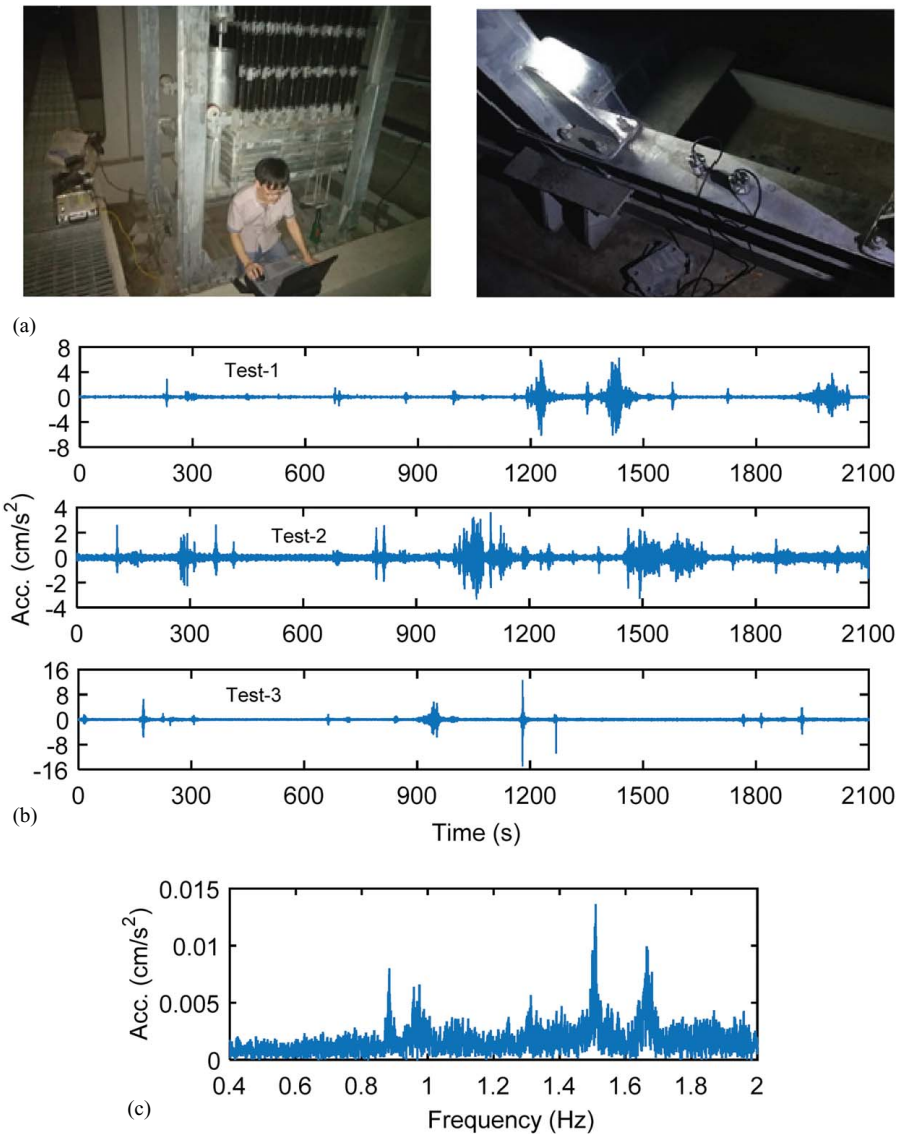

Fig. 12. Ambient vibration test: (a) field tests in August 2017; (b) three measured accelerations; and (c) Fourier spectrum of Test 1 between 0.4 and 2 Hz.

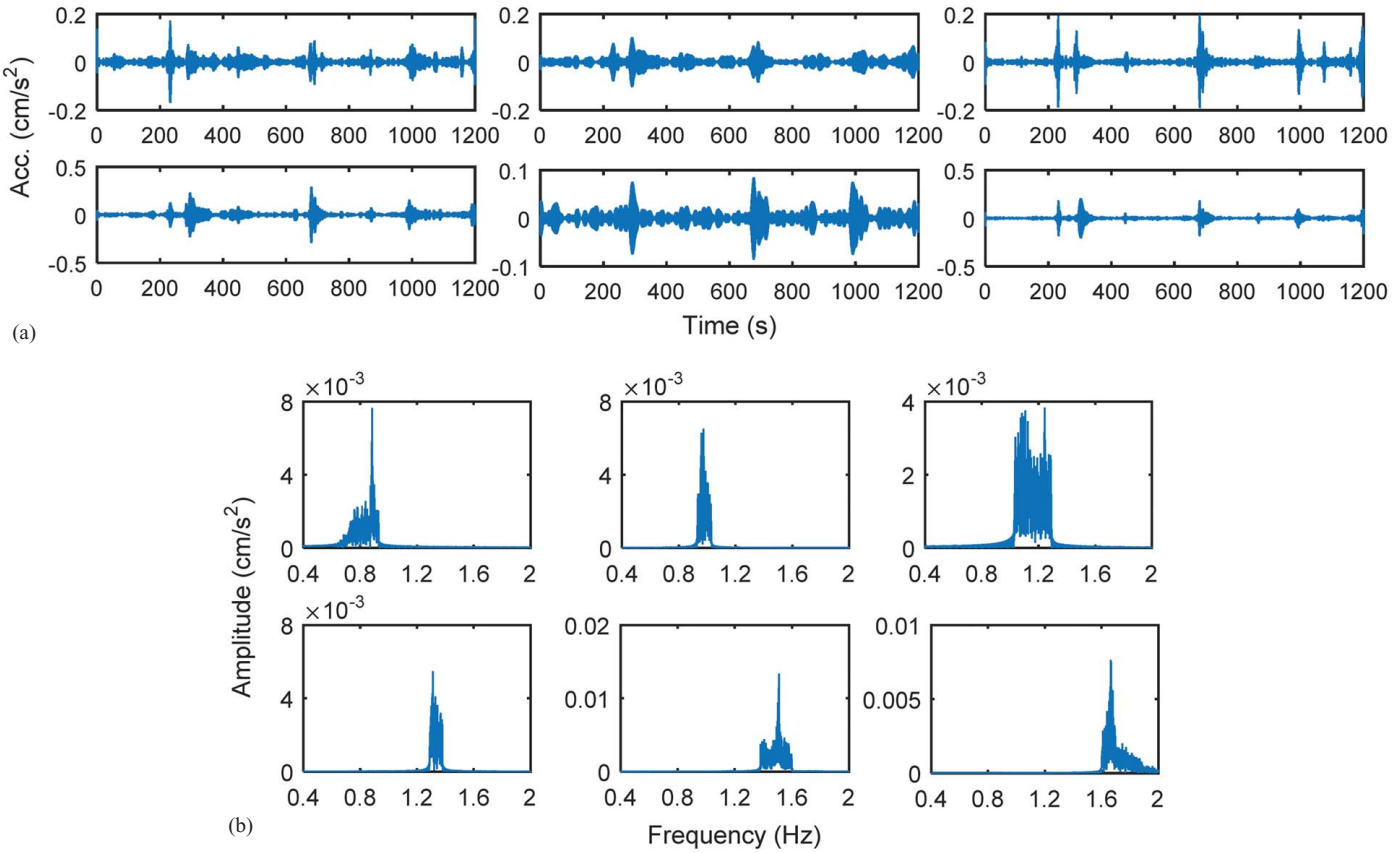

Fig. 13. AMD result of Test 1: (a) decomposed subsignals; and (b) Fourier spectra.

Table 1. Identified natural frequencies

Test	Mode 1	Mode 2			Mode 3			Mode 4	Mode 5	Mode 6
Natural frequency-1	0.898	0.977	1.055[a]	1.094[a]	1.172[a]	1.25[a]	1.289[a]	1.328	1.523	1.68
Natural frequency-2	0.898	0.977	1.055[a]	1.133[a]	1.172[a]	—	—	1.328	1.523	1.68
Natural frequency-3	0.898	0.977	1.016[a]	1.094[a]	—	1.211[a]	1.289[a]	1.328	1.523	1.68

[a]The identified natural frequency is ambiguous.

Table 2. Design parameters of the MRTMD and TMD

Design parameters	TMD			MRTMD		
	$\mu = 0.3\%$	$\mu = 0.5$	$\mu = 1\%$	$\mu = 0.3\%$	$\mu = 0.5\%$	$\mu = 1\%$
β	0.996	0.996	0.992	0.996	0.996	0.992
ξ_t	6%	7%	7.5%	6%	7%	7.5%
Number of MR damper	0	0	0	8	8	12

deviations are assumed to be 5% of the measurement standard deviations. The initial amplitude of the bridge is assumed as 30 mm.

Fig. 14 shows the comparison result between the TMD and MRTMD controls when $\mu = 0.3\%$. The mis means the ratio between ω_b and $\bar{\omega}_b$. Although the TMD has a better control effect than the MRTMD when the mis is 1, i.e., there is no detuning, and the MRTMD control can meet the requirement of the China code. When the mis are 0.94 and 1.06, the TMD fails in reducing the vortex-induced amplitude and the mass stroke is larger than 300 mm, but the MRTMD can prevent the amplitude from increasing with time and the mass stroke is smaller than 300 mm.

Fig. 15 shows the estimated frequency, force–displacement curve, control voltage, and control current of the MRTMD. The estimated frequencies after 20 s are basically the same as that before 20 s, indicating that the window method can accurately estimate the dominant vibration frequency. A good match between the desired control force and the MR damper force is observed, indicating that the MR damper force control scheme is feasible in determining the control voltage. The error between the desired control force and the MR damper force is caused by two reasons; the first is the clipped property of the MR damper force, and the second is the time delay and large updating time. It can be seen from Fig. 15(c) that the control voltage and current present a stairlike curve, not a smooth curve, indicating that the real-time tuning of the MRTMD is not sufficient. This is because the updating time of the control voltage is 0.1 s, which is a relatively large value for real-time tuning. The time delay means that the control current lags behind the control voltage due to the current driver dynamics, as shown in Fig. 15(c). In the case of mis = 1 and mis = 0.94, the control voltage is switched from low value to high value when the sign of $\dot{q}_t$ changes, and accordingly, the MR damper force could be close to the desired control force despite the time delay. In the case of mis = 1.06, the control voltage is switched from high value to low value when the sign of $\dot{q}_t$ changes, and accordingly, the MR damper generates a large force with an opposite sign due to the time delay.

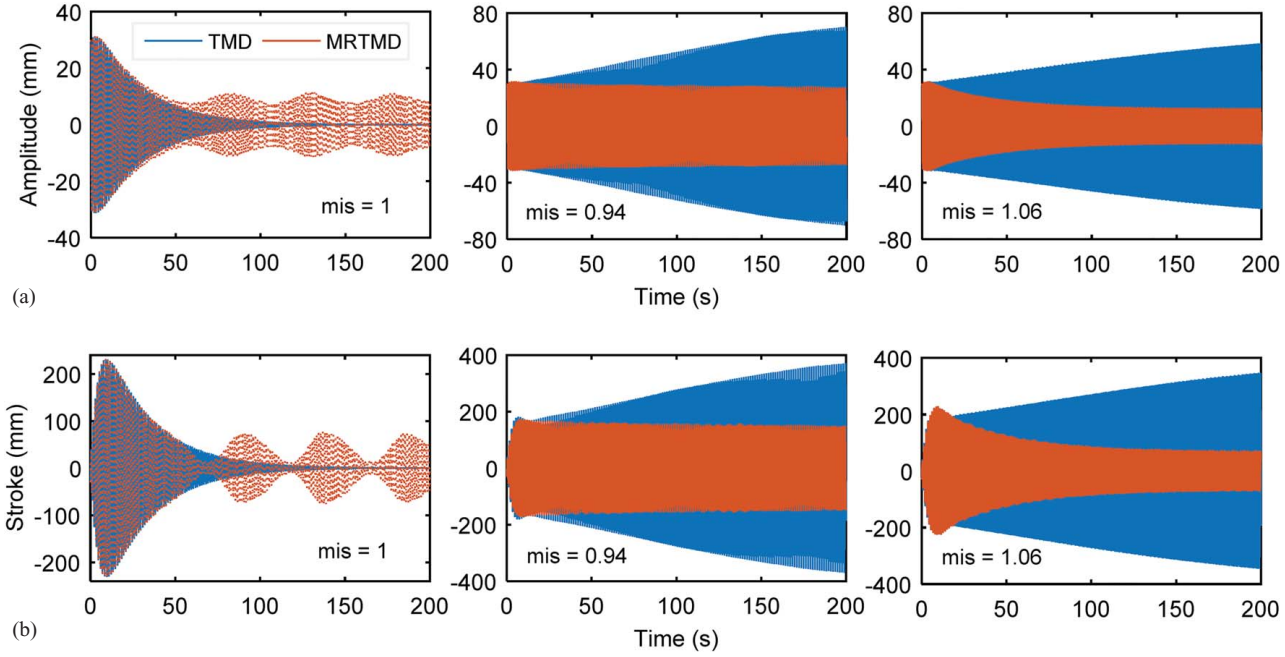

Fig. 14. Comparison of control results between the TMD and MRTMD when $\mu = 0.3\%$: (a) amplitude of the bridge; and (b) mass stroke.

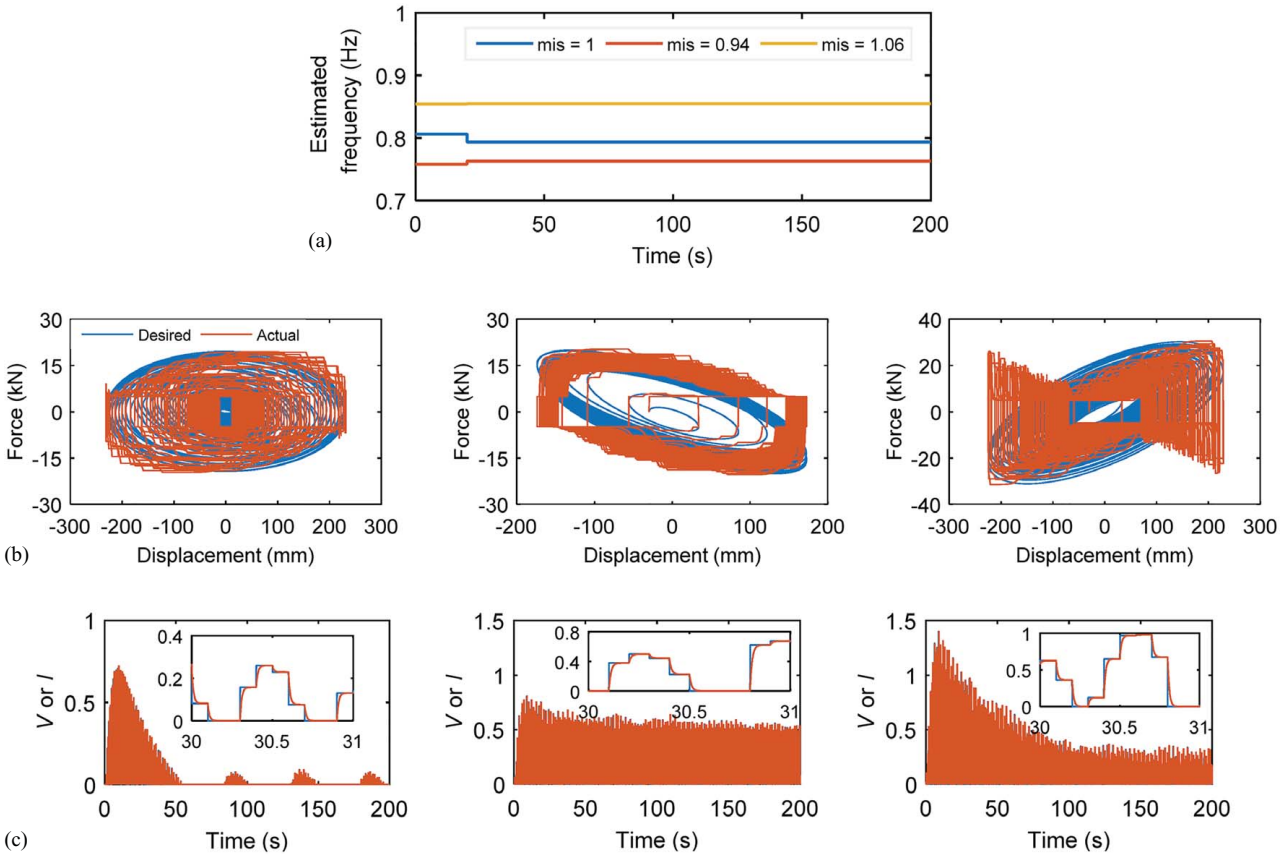

Fig. 15. Estimated frequency, force–displacement curve, and control voltage of the MRTMD: (a) estimated frequency; (b) force–displacement curve; and (c) control voltage.

Fig. 16 shows the comparison result between the TMD and MRTMD controls with varying mis when $\mu = 0.3\%$. If the vortex-induced amplitude is smaller than the initial amplitude 30 mm, we can consider that the negative damping ratio is eliminated, that is, to say, the VIV is well mitigated. Based on this criterion, we find that the TMD and MRTMD effectively mitigate the VIV when $0.96 \leq \text{mis} \leq 1.05$ and $0.94 \leq \text{mis} \leq 1.08$, respectively, which indicates that the MRTMD control has better robustness than the TMD

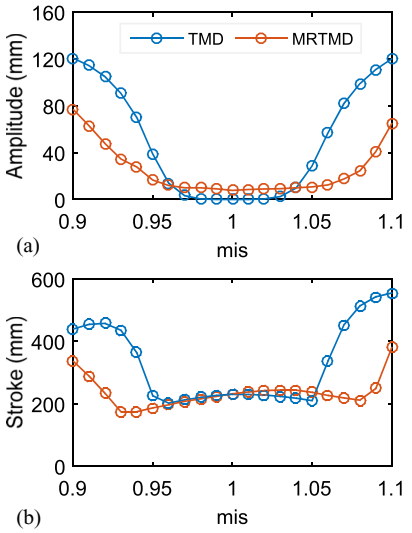

Fig. 16. Comparison between the TMD and MRTMD controls with varying mis when $\mu = 0.3\%$: (a) amplitude of the bridge; and (b) mass stroke.

control. Thanks to better robustness, the mass stroke of the MRTMD is much smaller than that of the TMD control when the mis greatly deviates from 1.

Effect of Frequency Estimation

Fig. 17 shows the effect of the offline estimation on the MRTMD control. In the MRTMD-1 control, the AMD method (offline estimation) is used within the first 20 s. In the MRTMD-2 control, the nominal natural frequency $\bar{\omega}_b$ is used within the first 20 s. It can be seen from Fig. 17(a) that the results of the vortex-induced amplitude and mass stroke in the two MRTMD controls are basically the same, which indicates that the effect of the offline estimation on the MRTMD control is small. It is noted that the vortex-induced amplitude here refers to the steady-state amplitude or the maximum amplitude between 198 and 200 s. Fig. 17(b) shows the comparison result within the first 70 s when mis = 1.06. It can be seen that MRTMD-1 has a better control effect than MRTMD-2, especially between 15 and 50 s. Because the offline estimation in the first 20 s makes the MRTMD be in a tuning state as soon as possible, and this advantage is significant in the severe detuning case. In general, the offline estimation can improve the tuning capability of the MRTMD.

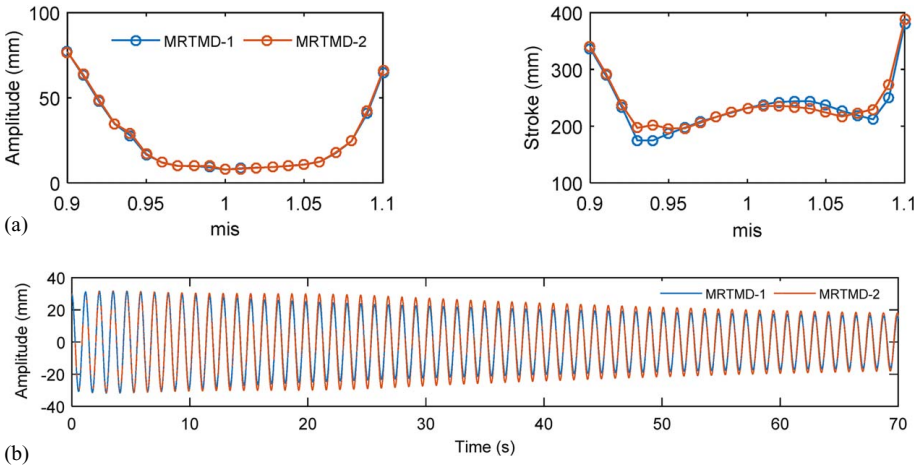

Fig. 17. Effect of offline estimation on the MRTMD control: (a) amplitude and stroke; and (b) amplitude during 0–70 s.

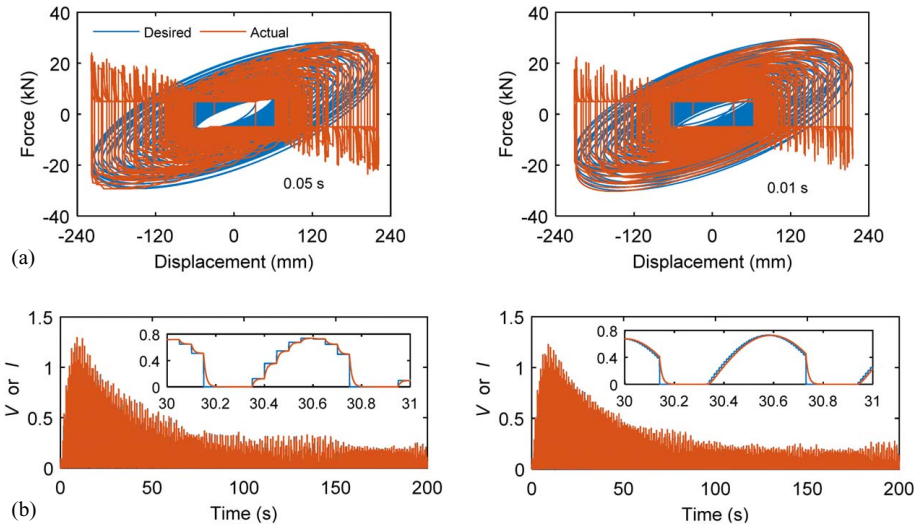

Fig. 18. Force–displacement curve and control voltage of the MRTMD with a different updating time: (a) force–displacement curve and updating time are 0.05 and 0.01 s; and (b) control voltage and updating time are 0.05 and 0.01 s.

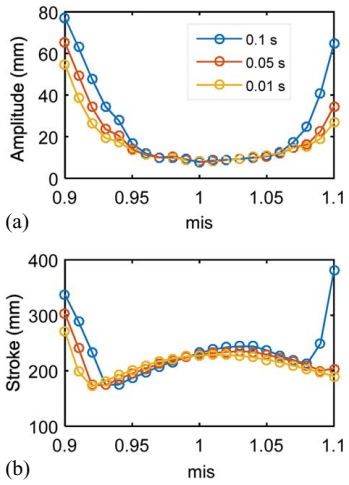

Fig. 19. Control result of the MRTMDs with a different updating time: (a) amplitude of the bridge; and (b) mass stroke.

Effect of Updating Time

In order to improve the real-time tuning, the updating time of the control voltage is reduced to 0.05 and 0.01 s. Fig. 18 shows the force–displacement curve, control voltage, and control current with a different updating time. The mis is assumed as 1.06 in Fig. 18. As the updating time decreases, the force–displacement curve becomes smoother, and the MR damper force is getting closer to the desired control force. Similarly, as the updating time decreases, the control voltage and current curves become smoother, and the two curves are more matched with each other. However, the control force error induced by the time delay still exists, because the parameter related to the time delay $\eta = 100$ is unchanged.

Fig. 19 shows the control result of the MRTMDs with a different updating time. The MRTMDs with the updating time of 0.1, 0.05, and 0.01 s can effectively mitigate the VIV when $0.94 \leq \text{mis} \leq 1.08$, $0.93 \leq \text{mis} \leq 1.09$, and $0.92 \leq \text{mis} \leq 1.1$, respectively, indicating that decreasing the updating time can improve the real-time tuning of the MRTMD. Also, decreasing the updating time can reduce the mass stroke, but the effect of the updating time on the mass

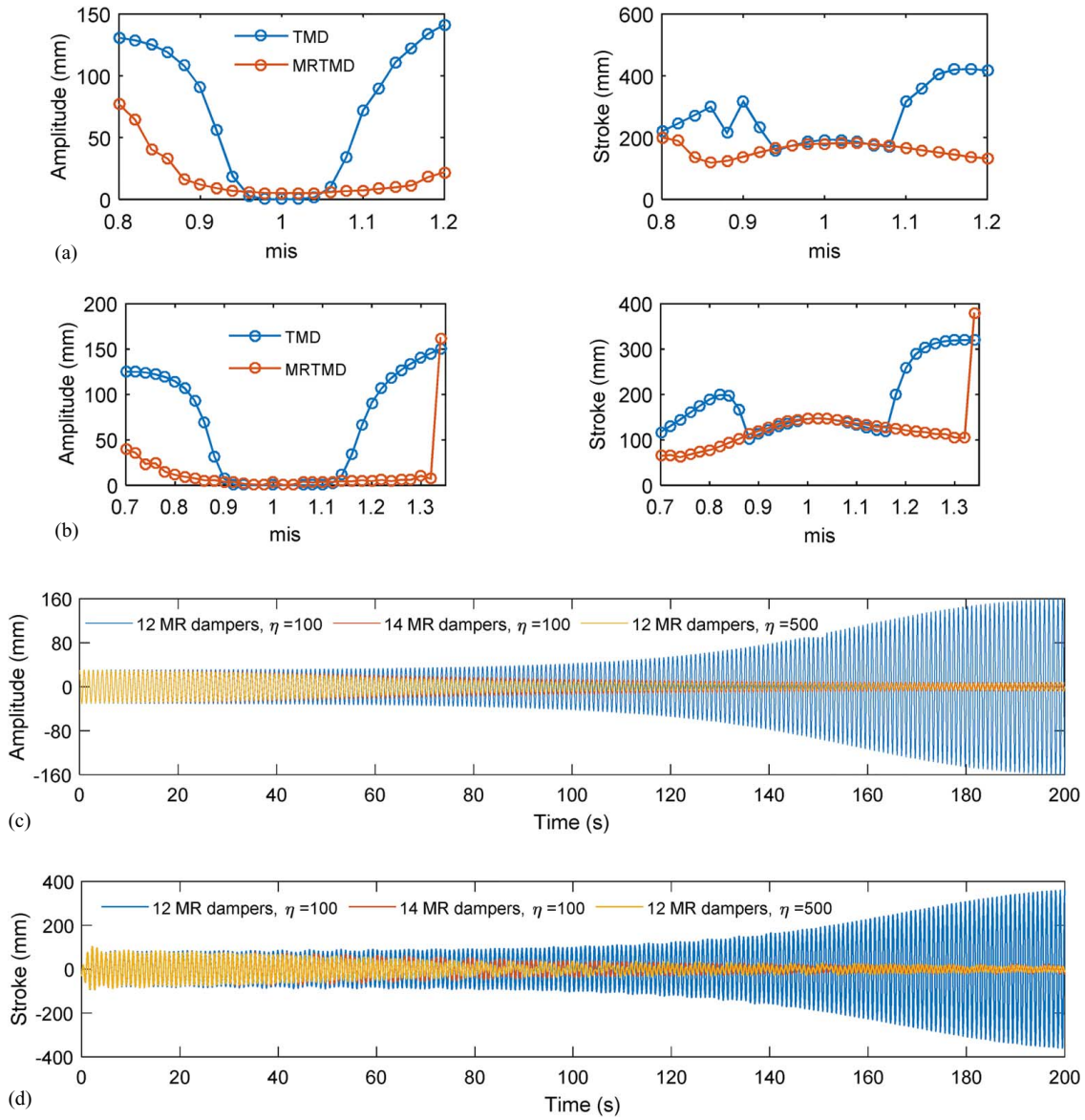

Fig. 20. Control result of the MRTMDs with different mass ratios: (a) $\mu = 0.5\%$; (b) $\mu = 1\%$; (c) amplitude when the mis is 1.34; and (d) stroke when the mis is 1.34.

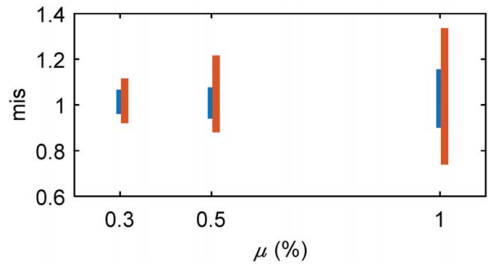

Fig. 21. Effective range of the mis of the MRTMDs with different mass ratios.

stroke reduction is not significant. In subsequent simulations, the updating time of the control voltage is designed as 0.01 s.

Effect of Mass Ratio

Although the MRTMD control is more robust than the TMD control, the improvement is not significant. This is because that the mass ratio used in simulations is too small to fully demonstrate the advantage of the MRTMD. Thus, we consider the other two mass ratios, $\mu = 0.5\%$ and $\mu = 1\%$. Fig. 20 shows the control result of the MRTMDs with different mass ratios. It can be seen that increasing the mass ratio can improve the robustness of the TMD and MRTMD controls. Furthermore, the advantage of the MRTMD in the robustness is more significant as the mass ratio increases. Besides, the mass stroke of the MRTMD is limited to less than 300 mm due to the good tuning capability of the MRTMD. It is noted that there are sudden increases in the amplitude and stroke of the MRMD when the mis is 1.34. There are two main reasons for the result; the first is that the desired control force is larger than the maximum force provided by 12 MR dampers when the mis is 1.34, and the second is that the dynamics involved in MR fluid reaching rheological equilibrium causes a sharp between the maximum negative force and zero force when the mis is larger than 1, as shown in Fig. 18(a). These two reasons together destroy the retuning of the MRTMD, and then the MRTMD becomes a conventional TMD. With increasing the number of MR damper or increasing the parameter η, the control effect of the MRTMD is improved and the mass stroke is less than 300 mm, as shown in Figs. 20(c and d).

Fig. 21 shows the effective range of the mis of the MRTMDs with different mass ratios. The effective range of the mis refers to the mis range with the vortex-induced amplitude is less than 300 mm. It can be seen that the effective ranges of the MRTMD are wider than those of the TMD within the three mass ratios; they are $0.96 \le \text{mis} \le 1.05$, $0.94 \le \text{mis} \le 1.06$, and $0.90 \le \text{mis} \le 1.14$ for the TMD control; and $0.91 \le \text{mis} \le 1.1$, $0.88 \le \text{mis} \le 1.2$, and $0.74 \le \text{mis} \le 1.32$ for the MRTMD control. For example, $0.74 \le \text{mis} \le 1.32$ means that the generalized stiffness for the first vertical-bending mode changes from 54.76% to 174. 24% of its nominal value according to $k = m\omega^2$; in other words, the MRTMD is robust enough in mitigating the VIV in bridges.

Conclusions

The paper presented a numerical study on the MRTMD control of the VIV in bridges. In order to realize the real-time tuning of the MRTMD, a reliable control strategy consisting of the control force design, control command determination, and frequency estimation was proposed. Based on the analytical stroke-amplitude ratio and the equivalent damping ratio, the desired control force was determined by considering the control effect and the mass stroke of the MRTMD in the VIV mitigation, simultaneously. A two-step strategy for the frequency estimation was used to improve the tuning capability of the MRTMD. Numerical simulations of a long-span continuous bridge under the VIV were performed to validate the superiority of the MRTMD control over the TMD control. The simulation results demonstrated that the MRTMD was more robust against the resonant frequency uncertainty than the TMD in the VIV mitigation, and the maximum mass stroke was less than a preset stroke in both tuned and mistuned cases. The two-step strategy can make the MRTMD be in a well-tuned state as soon as possible. Also, it was found that decreasing the updating time of the control voltage can improve the real-time tuning capability of the MRTMD. If the mis was larger than 1, the MRTMD cannot accurately emulate the control force with a positive stiffness due to the existence of the dynamics involved in MR fluid reaching rheological equilibrium.

Data Availability Statement

All of the data, models, or code that support the findings of this study are available from the corresponding author upon reasonable request.

Acknowledgments

This research was financially supported by the National Science Fund for Distinguished Young Scholars of China (51625803), National Natural Science Foundation of China (51878355), Program of Changjiang Scholars of Ministry of Education, Tencent Foundation through the XPLORER PRIZE, and Superiority Academic Discipline Construction Project of Jiangsu Higher Education Institutions (CE02-1-49).

References

Battista, R. C., and M. S. Pfeil. 2000. "Reduction of vortex-induced oscillations of Rio–Niterói Bridge by dynamic control devices." *J. Wind Eng. Ind. Aerodyn.* 84 (3): 273–288. https://doi.org/10.1016/S0167-6105(99)00108-7.

Chen, G., and Z. Wang. 2012. "A signal decomposition theorem with Hilbert transform and its application to narrowband time series with closely spaced frequency components." *Mech. Syst. Sig. Process.* 28: 258–279. https://doi.org/10.1016/j.ymssp.2011.02.002.

Christie, M. D., S. Sun, L. Deng, D. H. Ning, H. Du, S. W. Zhang, and W. H. Li. 2019. "A variable resonance magnetorheological-fluid-based pendulum tuned mass damper for seismic vibration suppression." *Mech. Syst. Sig. Process.* 116: 530–544. https://doi.org/10.1016/j.ymssp.2018.07.007.

Dai, J., Z. D. Xu, and P. P. Gai. 2020a. "Parameter determination of the tuned mass damper mitigating the vortex-induced vibration in bridges." *Eng. Struct.* 221: 111084. https://doi.org/10.1016/j.engstruct.2020.111084.

Dai, J., Z. D. Xu, P. P. Gai, and H. W. Li. 2020b. "Effect of frequency dependence of large mass ratio viscoelastic tuned mass damper on seismic performance of structures." *Soil Dyn. Earthquake Eng.* 130: 105998. https://doi.org/10.1016/j.soildyn.2019.105998.

Dai, J., Z. D. Xu, X. J. Yin, P. P. Gai, and Y. Luo. 2019. "Parameters design of TMD mitigating vortex-induced vibration of the Hong Kong–Zhuhai–Macao Bridge deep-water non-navigable bridge." *J. Bridge Eng.* 24 (8): 06019005. https://doi.org/10.1061/(ASCE)BE.1943-5592.0001450.

Dyke, S. J., B. F. Spencer, M. K. Sain, and J. D. Carlson. 1996. "Modeling and control of magnetorheological dampers for seismic response reduction." *Smart Mater. Struct.* 5 (5): 565–575. https://doi.org/10.1088/0964-1726/5/5/006.

Dyke, S. J., B. F. Spencer, M. K. Sain, and J. D. Carlson. 1998. "An experimental study of MR dampers for seismic protection." *Smart Mater. Struct.* 7 (5): 693–703. https://doi.org/10.1088/0964-1726/7/5/012.

Ehsan, F., and R. H. Scanlan. 1990. "Vortex-induced vibrations of flexible bridges." *J. Eng. Mech.* 116 (6): 1392–1411. https://doi.org/10.1061/(ASCE)0733-9399(1990)116:6(1392).

Fujino, Y., and Y. Yoshida. 2002. "Wind-induced vibration and control of Trans-Tokyo Bay Crossing bridge." *J. Struct. Eng.* 128 (8): 1012–1025. https://doi.org/10.1061/(ASCE)0733-9445(2002)128:8(1012).

Fujitani, H., H. Sakae, R. Kawasaki, H. Fujii, and T. Saito. 2008. "Verification of real-time hybrid tests of response control of base isolation system by MR damper comparing shaking table tests." *SPIE Int. Society Opt. Eng.* 6932: 69320Z. https://doi.org/10.1117/12.791079.

Jeon, S., and M. Tomizuka. 2007. "Benefits of acceleration measurement in velocity estimation and motion control." *Control Eng. Pract.* 15 (3): 325–332. https://doi.org/10.1016/j.conengprac.2005.10.004.

Kang, J., H. S. Kim, and D. G. Lee. 2011. "Mitigation of wind response of a tall building using semi-active tuned mass dampers." *Struct. Des. Tall Spec. Build.* 20 (5): 552–565. https://doi.org/10.1002/tal.609.

Kim, S., J. Park, and H. K. Kim. 2016. "Damping identification and serviceability assessment of a cable-stayed bridge based on operational monitoring data." *J. Bridge Eng.* 22 (3): 04016123. https://doi.org/10.1061/(ASCE)BE.1943-5592.0001004.

Laima, S., H. Li, W. Chen, and F. Li. 2013. "Investigation and control of vortex-induced vibration of twin box girders." *J. Fluids Struct.* 39: 205–221. https://doi.org/10.1016/j.jfluidstructs.2012.10.009.

Larsen, A. 1995. "A generalized model for assessment of vortex-induced vibrations of flexible structures." *J. Wind Eng. Ind. Aerodyn.* 57 (2–3): 281–294. https://doi.org/10.1016/0167-6105(95)00008-F.

Larsen, A., S. Esdahl, J. E. Andersen, and T. Vejrum. 2000. "Storebælt suspension bridge—Vortex shedding excitation and mitigation by guide vanes." *J. Wind Eng. Ind. Aerodyn.* 88 (2–3): 283–296. https://doi.org/10.1016/S0167-6105(00)00054-4.

Larsen, A., E. Svensson, and H. Andersen. 1995. "Design aspects of tuned mass dampers for the Great Belt East Bridge approach spans." *J. Wind Eng. Ind. Aerodyn.* 54–55: 413–426. https://doi.org/10.1016/0167-6105(94)00057-K.

Li, H., S. Laima, Q. Zhang, N. Li, and Z. Liu. 2014. "Field monitoring and validation of vortex-induced vibrations of a long-span suspension bridge." *J. Wind Eng. Ind. Aerodyn.* 124: 54–67. https://doi.org/10.1016/j.jweia.2013.11.006.

Liao, H. L. 2013. "Experimental study on wind-induced vibration Hong Kong–Zhuhai–Macao Bridge." [In Chinese.] In *Proc., 16th National Conf. on Structural Wind Engineering*, 35–42. Cheng Du, China: Southwest Jiaotong Univ.

Macdonald, J. H. G., P. A. Irwin, and M. S. Fletcher. 2002. "Vortex-induced vibrations of the Second Severn Crossing cable-stayed bridge—Full-scale and wind tunnel measurements." *Proc. Inst. Civ. Eng. Struct. Build.* 152 (2): 123–134. https://doi.org/10.1680/stbu.2002.152.2.123.

Magalhães, F., E. Caetano, and Á Cunha. 2007. "Challenges in the application of stochastic modal identification methods to a cable-stayed bridge." *J. Bridge Eng.* 12 (6): 746–754. https://doi.org/10.1061/(ASCE)1084-0702(2007)12:6(746).

Maślanka, M. 2019. "Optimised semi-active tuned mass damper with acceleration and relative motion feedbacks." *Mech. Syst. Sig. Process.* 130: 707–731. https://doi.org/10.1016/j.ymssp.2019.05.025.

Ministry of Communication of PRC. 2019. *Wind-resistant design specification for highway bridges*. [In Chinese.] JTG/T 3360-01-2018. Beijing: China Communications Press.

Nagarajaiah, S. 2009. "Adaptive passive, semiactive, smart tuned mass dampers: Identification and control using empirical mode decomposition, Hilbert transform, and short-term Fourier transform." *Struct. Control Health Monit.* 16 (7–8): 800–841. https://doi.org/10.1002/stc.349.

Nagarajaiah, S., and N. Varadarajan. 2005. "Short time Fourier transform algorithm for wind response control of buildings with variable stiffness TMD." *Eng. Struct.* 27 (3): 431–441. https://doi.org/10.1016/j.engstruct.2004.10.015.

Owen, J. S., A. M. Vann, J. P. Davies, and A. Blakeborough. 1996. "The prototype testing of Kessock bridge: Response to vortex shedding." *J. Wind Eng. Ind. Aerodyn.* 60: 91–108. https://doi.org/10.1016/0167-6105(96)00026-8.

Qin, H., H. L. Liao, M. S. Li, and Y. G. Sun. 2013. "Vortex-induced vibration of continuous beam bridge and its mitigation." In *Proc., 8th Asia-Pacific Conf. on Wind Engineering*, 469–477. Chennai, India: CSIR-Structural Engineering Research Centre.

Setareh, M., J. K. Ritchey, T. M. Murray, J. Koo, and M. Ahmadian. 2007. "Semi-active tuned mass damper for floor vibration control." *J. Struct. Eng.* 133 (2): 242–250. https://doi.org/10.1061/(ASCE)0733-9445(2007)133:2(242).

Shi, W., L. Wang, and Z. Lu. 2018. "Study on self-adjustable tuned mass damper with variable mass." *Struct. Control Health Monit.* 25 (3): e2114. https://doi.org/10.1002/stc.2114.

Shi, Y., T. C. Becker, S. Furukawa, E. Sato, and M. Nakashima. 2014. "LQR control with frequency-dependent scheduled gain for a semi-active floor isolation system." *Earthquake Eng. Struct. Dyn.* 43 (9): 1265–1284. https://doi.org/10.1002/eqe.2352.

Siringoringo, D. M., and Y. Fujino. 2007. "Dynamic characteristics of a curved cable-stayed bridge identified from strong motion records." *Eng. Struct.* 29 (8): 2001–2017. https://doi.org/10.1016/j.engstruct.2006.10.009.

Sun, C., and S. Nagarajaiah. 2014. "Study on semi-active tuned mass damper with variable damping and stiffness under seismic excitations." *Struct. Control Health Monit.* 21 (6): 890–906. https://doi.org/10.1002/stc.1620.

Sun, Z., Z. L. Zhou, Y. Y. Ying, and X. Q. Li. 2020. "Tuned mass dampers for wind-induced vibration control of Chongqi Bridge." *J. Bridge Eng.* 25 (1): 05019014. https://doi.org/10.1061/(ASCE)BE.1943-5592.0001510.

Wang, L., W. Shi, and Y. Zhou. 2019. "Study on self-adjustable variable pendulum tuned mass damper." *Struct. Des. Tall Spec. Build.* 28 (1): e1561. https://doi.org/10.1002/tal.1561.

Wang, Z., and G. Chen. 2014. "Analytical mode decomposition with Hilbert transform for modal parameter identification of buildings under ambient vibration." *Eng. Struct.* 59: 173–184. https://doi.org/10.1016/j.engstruct.2013.10.020.

Weber, F. 2013a. "Bouc–Wen model-based real-time force tracking scheme for MR dampers." *Smart Mater. Struct.* 22 (4): 045012. https://doi.org/10.1088/0964-1726/22/4/045012.

Weber, F. 2013b. "Dynamic characteristics of controlled MR-STMDs of Wolgograd Bridge." *Smart Mater. Struct.* 22 (9): 095008. https://doi.org/10.1088/0964-1726/22/9/095008.

Weber, F. 2014. "Semi-active vibration absorber based on real-time controlled MR damper." *Mech. Syst. Sig. Process.* 46 (2): 272–288. https://doi.org/10.1016/j.ymssp.2014.01.017.

Weber, F., and M. Maślanka. 2012. "Frequency and damping adaptation of a TMD with controlled MR damper." *Smart Mater. Struct.* 21 (5): 055011. https://doi.org/10.1088/0964-1726/21/5/055011.

Weber, F., and M. Maślanka. 2014. "Precise stiffness and damping emulation with MR dampers and its application to semi-active tuned mass dampers of Wolgograd Bridge." *Smart Mater. Struct.* 23 (1): 015019. https://doi.org/10.1088/0964-1726/23/1/015019.

Wen, Q., X. G. Hua, Z. Q. Chen, H. W. Niu, and X. Y. Wang. 2018. "AMD-based random decrement technique for modal identification of structures with close modes." *J. Aerosp. Eng.* 31 (5): 04018057. https://doi.org/10.1061/(ASCE)AS.1943-5525.0000882.

Wu, T., and A. Kareem. 2013. "Vortex-induced vibration of bridge decks: Volterra series-based model." *J. Eng. Mech.* 139 (12): 1831–1843. https://doi.org/10.1061/(ASCE)EM.1943-7889.0000628.

Wu, W. J., and C. S. Cai. 2007. "Theoretical exploration of a taut cable and a TMD system." *Eng. Struct.* 29 (6): 962–972. https://doi.org/10.1016/j.engstruct.2006.07.009.

Xu, Y. L., J. M. Ko, and W. S. Zhang. 1997. "Vibration studies of Tsing Ma suspension bridge." *J. Bridge Eng.* 2 (4): 149–156. https://doi.org/10.1061/(ASCE)1084-0702(1997)2:4(149).

Yang, G., B. F. Spencer, Jr., J. D. Carlson, and M. K. Sain. 2002. "Large-scale MR fluid dampers: Modeling and dynamic performance considerations." *Eng. Struct.* 24 (3): 309–323. https://doi.org/10.1016/S0141-0296(01)00097-9.

Zemp, R., J. C. D. La Llera, and J. L. Almazan. 2011. "Tall building vibration control using a TM-MR damper assembly." *Earthquake Eng. Struct. Dyn.* 40 (3): 339–354. https://doi.org/10.1002/eqe.1033.

Zemp, R., J. C. D. La Llera, H. Saldias, and F. Weber. 2016. "Development of a long-stroke MR damper for a building with tuned masses." *Smart Mater. Struct.* 25 (10): 105006. https://doi.org/10.1088/0964-1726/25/10/105006.